Structure, Vibrational Spectra, and Unimolecular Dissociation of Gaseous 1-Fluoro-1-phenethyl Cations

Jos Oomens,[†] Elfi Kraka,[‡] Michael K. Nguyen,[§] and Thomas Hellman Morton*[,§]

FOM Institute for Plasmaphysics Rijnhuizen, Edisonbaan 14, NL-3438 MN Nieuwegein, The Netherlands, Department of Chemistry, University of the Pacific, Stockton, California 95211, and Department of Chemistry, University of California, Riverside, California 92521-0403

Received: May 28, 2008; Revised Manuscript Received: July 15, 2008

The multiple CF bond character of $PhCFMe^+$ ions has been examined by means of theory, vibrational spectroscopy of the gaseous ions, and unimolecular decomposition chemistry. Atoms in Molecules analysis of DFT wave functions gives a CF bond order of $n = 1.25$ (as compared with $n = 1.38$ for Me_2CF^+, relative to $n = 1$ for fluoromethane and $n = 2$ for diatomic CF^+), which is consistent with calculations of adiabatic CF stretching frequencies (ν_{CF}). Experimental gas phase IR spectra, recorded by means of resonant multiphoton dissociation (IRMPD) using a free-electron laser connected to an FTICR mass spectrometer, show good agreement with predicted band positions for five deuterated isotopomers of $PhCFMe^+$. Metastable ion decompositions of deuterated analogues of $PhCFMe^+$ show the same HF/DF loss patterns as those produced by IRMPD. The evidence supports the conclusion that PhCFMe ions retain structural integrity until they become sufficiently excited to dissociate, whereupon they undergo intramolecular hydrogen scrambling that is competitive with HF/DF expulsion. Relative rates of hydrogen transposition and unimolecular dissociation are extracted from relative experimental fragment ion abundances. The predominant decomposition pathway is inferred to operate via a five-center transition state, as opposed to a four-center transition state for HF loss from gaseous Me_2CF^+.

Introduction

Direct attachment of fluorine to an electron-deficient carbon contributes to the net stabilization of a positive charge. Back-bonding from a lone pair to a vacant p orbital compensates for the electronegativity of the halogen. This π donation confers partial double-bond character upon the carbon−fluorine bond in cations.[1,2] That effect accounts for the gas-phase basicity of fluoroethylene[3] as well as the enhanced reactivity of vinyl fluorides toward electrophilic attack[4] and the observed shortening of the CF bond length in simple carbocations such as $(CH_3)_2CF^+$ (**1**).[5]

As structures **1a** and **1b** depict in Chart 1, an α-monofluorinated cation can be viewed as a resonance hybrid,[2] which is isoelectronic with the resonance structures that are conventionally drawn for simple carbonyl compounds.[6] Carbocations of this nature can be depicted as though they possess carbon−fluorine double bonds, as illustrated for ions **2** and **3**. These Lewis structures represent every atom with a complete octet.

Vibrational spectroscopy provides one measure of bond order. The X-ray structure of a crystalline salt of **1** shows the association between the cation and its counterions[5] that interferes with a meaningful assessment of CF bonding. In the gas phase, however, the absence of counterions permits a comparison of CF stretching frequencies with theoretical predictions. A variety of mass spectrometric techniques have lately become available that permit one to infer the vibrational spectra of isolated ions. Recently, we reported IR absorptions of gaseous carbocations

CHART 1

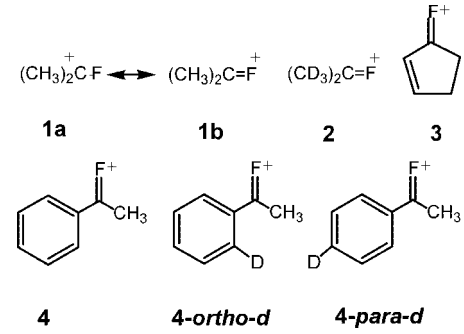

in which a single fluorine atom is directly attached to the sp^2 center that bears the positive charge.[7] The band assigned to the CF stretch in the simplest example studied, ion **2**, occurs around 1425 cm^{-1}.

The IR bands of gaseous **2** and **3** were recorded by observing their resonant multiphoton dissociation (IRMPD) action spectra by using a free-electron laser to irradiate ions trapped in an ICR cell.[7,8] Excitation leads to the unimolecular expulsion of neutral DF or HF, respectively, which is monitored by mass spectrometry as a function of wavelength. The $>C{=}F^+$ stretch has a force constant that is approximately 60% as large as that of an isolated ketone carbonyl, in accordance with predictions based on density functional theory (DFT). The calculated force constants for **2** and **3** have virtually the same values.

In condensed phases, α-monofluorinated cations can be generated by fluoride abstraction from a *gem*-difluoroalkane or by electrophilic attack of a vinyl fluoride. In the gas phase, two other avenues become available, as eqs 1 and 2 illustrate: electron ionization (EI) of a *tert*-alkyl fluoride followed by the

* To whom correspondence should be addressed. E-mail: morton@citrus.ucr.edu.
† FOM Institute for Plasmaphysics Rijnhuizen.
‡ University of the Pacific.
§ University of California.

10.1021/jp804706z CCC: $40.75
Published on Web 10/03/2008

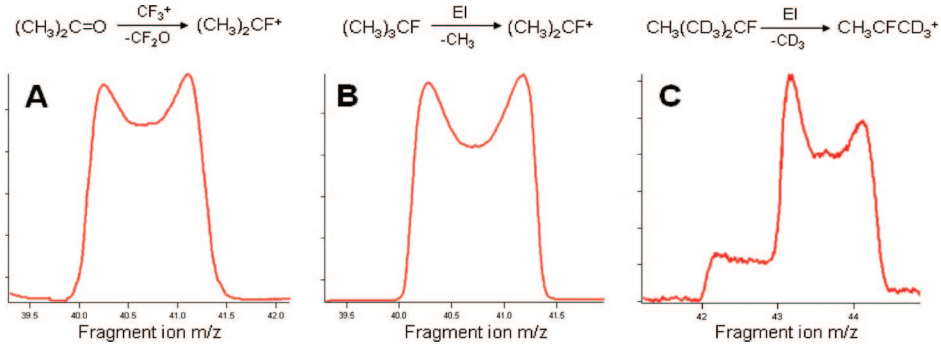

Figure 1. MIKES metastable peak profiles for HF expulsion from ion **1** and for HF and DF from **1-*d*$_3$**.[12]

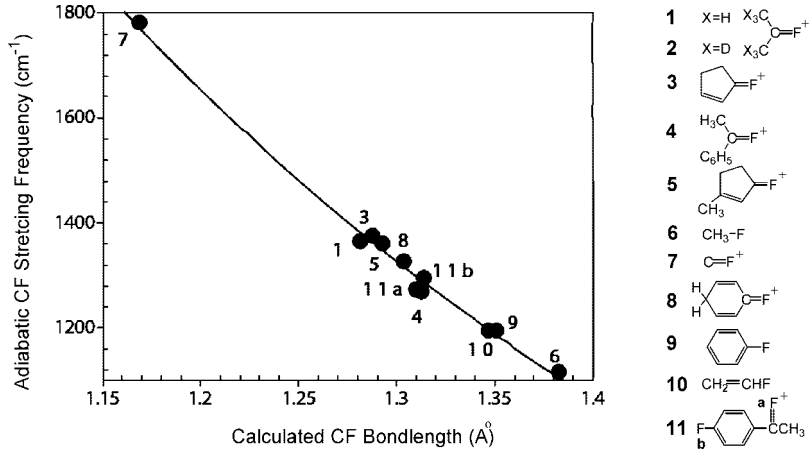

Figure 2. Adiabatic harmonic DFT CF stretching modes (ν_{CF}) versus calculated CF bond length.

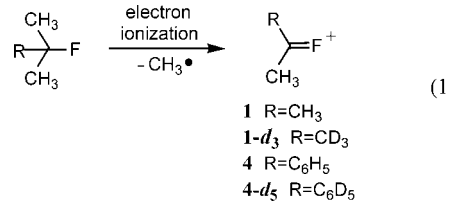

1 R=CH$_3$
1-*d*$_3$ R=CD$_3$
4 R=C$_6$H$_5$
4-*d*$_5$ R=C$_6$D$_5$ (1)

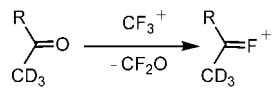

2 R=CD$_3$
4-*d*$_3$ R=C$_6$H$_5$ (2)

loss of an alkyl radical[9] or metathesis of a carbonyl compound with a perfluoroalkyl cation.[10] The structure of gaseous **1** has been confirmed by collection of neutral products from its bimolecular ion−molecule reactions, and experimental evidence rules out any detectable transposition of its carbons or hydrogens.[11] Unimolecular dissociation of **1** takes place via the loss of a molecule of neutral HF, for which the translational kinetic-energy release is the nearly same, regardless of whether **1** was produced by eq 1 or 2. Figure 1 reproduces the profiles for metastable ion decompositions of gaseous **1** via HF expulsion to give $C_3H_5^+$ ions as well as of **1-*d*$_3$**, which expels both HF and DF in a ratio of approximately 4:1.[12] The dish-topped peaks indicate a large translational kinetic-energy release that is consistent with what would be expected for a concerted four-center elimination.

This article explores the structure and unimolecular reactivity of a >C=F$^+$ bond when it is conjugated with a benzene ring. The analogy between isoelectronic >C=F$^+$ and >C=O becomes less apparent when charge can delocalize into an extended π system. In principle, a >C=F$^+$ bond should become weaker because of conjugation, just like a carbonyl group. However, as noted above, the comparison of **2** and **3** gives no evidence of such an interpretation.

The present study focuses on ion **4**, PhCFMe$^+$, which is isoelectronic with acetophenone, PhCOMe. First, we use theory to compare bonding in >C=F$^+$ with other CF bonds. Then, we present experimental data for unimolecular dissociation of **4** and deuterated analogues and compare metastable ion mass spectrometry with IRMPD results. Finally, we describe DFT potential-energy surfaces that provide an interpretation of the experimental results and analyze them accordingly.

As will be described later, theoretical analysis indicates a looser CF bond in **4**, as compared with that in **1**. Because the vibrational spectrum of gaseous fluorinated carbocations makes use of resonant MPD-induced expulsion of HF, the pathway for this expulsion has potential relevance. The theoretical results raise the question of whether the barrier to HF elimination from **4** becomes lower as a consequence of the weaker bond. Although the experiment provides a prima facie picture that is consistent with that supposition, as will be discussed below, a deeper exploration (including IRMPD spectra of four deuterated analogues of **4**) leads to an opposite conclusion and indicates that the principal pathways for HF expulsion from **1** and **4** take place via different types of transition state.

Results

CF Stretching Frequencies. Unlike carbonyl stretches, which do not couple extensively with other vibrations, the animation of calculated normal modes indicates that CF stretching participates to a significant degree in more than one normal mode, which makes a description of the CF bonds in terms of normal modes difficult. Therefore, the CF bonds are characterized in this work by localized adiabatic modes that are derived

TABLE 1: Bond Critical Point Electron Density (ρ_{BCP}), Bond Order (n),[a] CF Bond Length (r_{CF}), Calculated Adiabatic Harmonic CF Stretching Frequency (ν_{CF}), and Prediction of ν_{CF} from Equation 4 at B3LYP/6-31G**

	electron density (ρ_{BCP})	bond order (n)	bond length (r_{CF})	frequency (ν_{CF})	
				calcd	pred
1 $Me_2C{=}F^+$	0.305	1.379	1.282	1365	1382
3 *cyclo*-$C_5H_6F^+$	0.0299	1.343	1.288	1376	1365
4 $PhCFMe^+$	0.284	1.251	1.310	1273	1299
5 3-methyl-*cyclo*-$C_5H_6F^+$	0.297	1.328	1.293	1359	1350
6 MeF	0.239	1.00	1.383	1116	1107
7 $C{=}F^+$	0.395	2.00	1.169	1782	1772
8 p-protonated fluorobenzene	0.289	1.281	1.304	1325	1318
9 fluorobenzene	0.254	1.079	1.351	1195	1188
10 $CH_2{=}CHF$	0.255	1.087	1.347	1195	1197
11 *p*-$FC_6H_4CFCH_3^+$					
CH_3CF (**a**)	0.282	1.243	1.312	1268	1293
ring CF (**b**)	0.281	1.235	1.314	1295	1287
2-fluoropropane	0.224	0.920	1.405	1037	1055
t-butyl fluoride	0.177	0.785	1.416	1001	1030

[a] Using $n = B \exp[A\rho_{BCP} - 1]$, where $A = 2.2$ and $B = 1.444$.

from the adiabatic mode concept of Cremer, Kraka, and Konkoli.[13,14] Adiabatic modes are localized vibrations obtained by perturbing a leading parameter (such as a bond length, bond angle, dihedral angle, etc.) while relaxing all other geometrical parameters of the molecule. As has been shown by Cremer et al.,[13,15,16] the properties of adiabatic modes are well suited to describe a chemical bond and to analyze empirical rules between bond properties (e.g., Badger's rule[17]). Adiabatic modes represent an elaboration of the approach previously used to evaluate Hooke's law spring constants for ions **1** and **3**.[7]

The dissection into adiabatic modes can be applied to either calculated or experimental frequencies. In the present case, a set of molecules with CF bonds was chosen for which the observed vibrational frequencies agree with those calculated by DFT (taking into account anharmonic corrections). Figure 2 plots a data set that ranges from fluoromethane[19] to diatomic CF^+ (the ground-state singlet of which exhibits an experimental harmonic component of 1793 cm^{-1}[20] versus a calculated value of 1783 cm^{-1}). For example, the 12 fundamentals that were calculated for fluoroethylene at B3LYP/6-31G** (with anharmonic corrections) differ from the reported experimental frequencies by 0.6%, on average.[21] The level of agreement in the selected set of compounds warrants the dissection of CF stretching components out of their calculated harmonic normal modes. Table 1 summarizes the results, and Figure 2 plots adiabatic harmonic CF stretching frequencies versus calculated CF bond lengths for species whose infrared frequencies are available. Table 1 compares the calculated adiabatic values of ν_{CF} with those predicted on the basis of the correlation with bond length summarized in Figure 2.

Given a set of adiabatic frequencies for which the reduced mass remains constant, Badger's rule[17] suggests the following empirical relationship between equilibrium bond length (r_{CF}) and CF stretch

$$\nu_{CF} = a[r_{CF} - b]^{-3/2} \quad (3)$$

In the present instance, an exponential relation provides a much better fit for the data summarized in Figure 2 ($r^2 > 0.99$).

$$\nu_{CF} = 23260e^{-2.202 r_{CF}} \quad (4)$$

Because experimental bond lengths are not available for all of the entries in Table 1, B3LYP/6-31G** values of r_{CF} were used as well as the harmonic frequencies computed at that level.

The degree to which bond length correlates with CF stretch supports the inference that adiabatic ν_{CF} modes provide a measure of CF bond strength. The CF bond in ion **4** has both a lower adiabatic stretch and a longer bond than any of the other fluorinated cations. By contrast, the CF stretch of **3** scarcely differs from that of **1** or **2**.

Equation 4 leads to the set of predicted values for ν_{CF} summarized in Table 1. The table also includes the DFT bond order n, which was calculated using the atoms-in-molecules (AIM) topological analysis of ρ_{BCP}, the electron density at the bond critical point. AIM bond order calculations require calibration for two points for which we take the bond order of the C−F single bond in fluoromethane to be $n = 1$ and the bond order in the diatomic CF^+ ion to have the value $n = 2$. The CF^+ ion and carbon monoxide are isoelectronic, and bond orders as high as $n = 3$ have been assigned to both diatomics.[22] Ab initio calculations, by contrast, give Wiberg bond indices (natural atomic orbital basis) for diatomic CF^+ that are on the order of 1.6 to 1.65 times as great as those for fluoromethane. Assignment of $n = 2$ for diatomic CF^+ seems like a reasonable compromise.

Table 1 compares values of ν_{CF} predicted by eq 4 with the calculated adiabatic CF stretching frequencies not only for the species in Figure 2 (to which eq 4 was fitted) but also for cases in which AIM bond orders are calculated to have values of $n < 1$. For instance, the equilibrium CF bond length calculated for *tert*-butyl fluoride has a value that is not far from the experimental value ($r_{CF} = 1.43$ Å) determined by microwave spectroscopy[23] and an adiabatic stretching frequency (ν_{CF}) that is much lower than that of any of the other entries. These examples illustrate the reliability with which eq 4 can be extrapolated.

Metastable Ion Decompositions. The conclusion that **4** possesses a looser CF bond than does **2** or **3** suggests a comparison of peak profiles that uses mass-analyzed ion kinetic-energy (MIKE) spectrometry. The deuterated analogues lose both HF and DF. Unlike the dish-topped peaks in Figure 1 (for which the translational kinetic-energy release is on the order of 1 eV), the metastable ion profiles reproduced in Figure 3 exhibit composite peak shapes: large Gaussian peaks ($T_{0.5} = 0.03$ eV) on top of barely discernible dish-topped peaks. Best-fit Gaussian peak profiles (shown in blue in Figure 3) leave tails that indicate the presence of a small component with a large translational kinetic-energy release. The much lower translational kinetic-energy releases seen for the major metastable ion decompositions of **4** and its deuterated analogues (as compared with those of **1** and its d_3 analogue in Figure 1) support the inference that the major pathway for HF expulsion from **4** encounters a lower barrier.

However, two features cloud the picture. First, the superposition of a major Gaussian peak upon a much smaller dish-topped peak implies two different dissociation pathways. Does that mean there is more than one ion structure present? Second, the deuterated analogues expel both HF and DF, which amplifies this question. Moreover, a greater proportion of hydrogen seems to be coming from the ring than from the methyl group.

IRMPD Spectra. To address the issue of ion identity, IRMPD spectra were recorded for ion **4** and its deuterated analogues. Figure 4 compares experimental and calculated vibrational spectra for **4**, **4**-d_3, and **4**-d_5. Calculated spectra

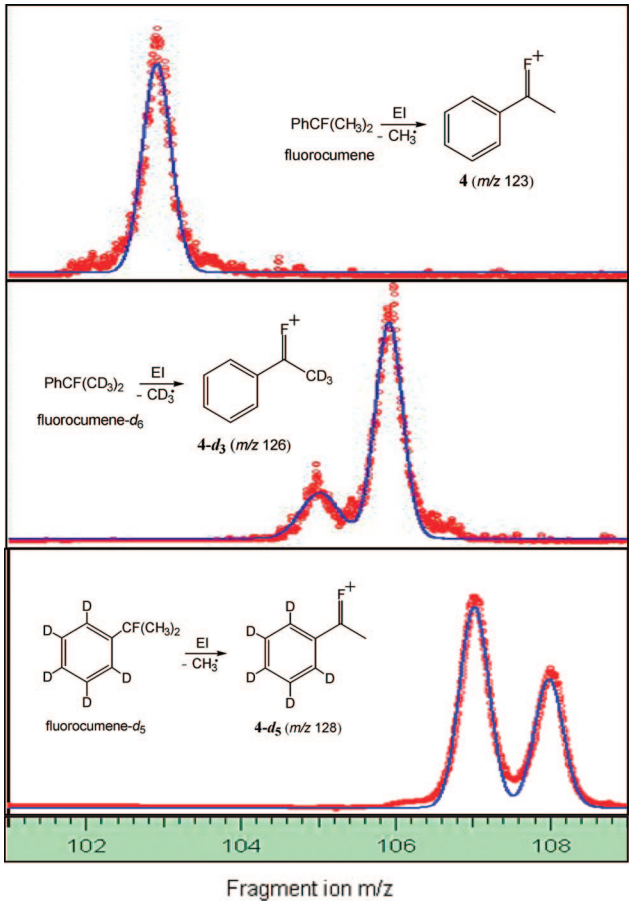

Figure 3. MIKE spectra (in red) of metastable ion decompositions of **4**, **4**-d_3, and **4**-d_5 produced by EI of the corresponding fluorocumenes. Blue curves show best-fit Gaussian peak profiles to the data.

(which include anharmonic corrections) show good agreement with experiment, and extraneous peaks, which would be anticipated if another ion was present, do not occur.

More importantly, the deuterated analogues exhibit both HF and DF loss. The IRMPD spectrum in Figure 4E compares the frequency dependence of the two pathways for **4**-d_5 and shows them to give virtually identical profiles. As in the MIKE spectrum of **4**-d_5 in Figure 3C, more DF loss takes place than HF loss.

Given that IRMPD indicates the presence of only one ion, the expulsion of both HF and DF admits two possible interpretations: either the isotopic label scrambles or ion **4** accesses more than one dissociation pathway. Whereas those two alternatives need not be mutually exclusive, Figure 5 reproduces the IRMPD of the two isomeric monodeuterated analogues of **4** drawn in Chart 1. These spectra exhibit differences sufficient to demonstrate that the two isomers retain distinct identities, but scrambling takes place after activation, which equilibrates them before they decompose.

The para isomer, **4**-*para*-*d*, has a calculated symmetrical, in-plane CH bending mode at 1206 cm^{-1} (which would correspond to an A_1 vibration if free rotation around the Ph−CF single bond effectively gave the ion C_{2v} symmetry). That prediction agrees well with the observed band at 1190 cm^{-1} in the experimental spectrum. IRMPD of the ortho isomer, **4**-*ortho*-*d*, displays a different absorption spectrum including a much smaller band at that frequency. Experimental and calculated spectra show good agreement. The comparison of the two experimental spectra demonstrates that the deuterated ions retain the label positions of their neutral precursors and do not scramble hydrogen and deuterium until after excitation.

IRMPD of both monodeuterated ions leads to proportions of HF and DF loss that are parallel to one another. Therefore, isotopic scrambling must take place after the ions acquire enough internal energy to dissociate. In all likelihood, a single pathway for HF expulsion gives rise to the Gaussian peaks in the MIKE spectrum of **4**, and the occurrence of both HF and DF loss in the deuterated analogues results from scrambling in the activated ions.

Theoretical Considerations. The potential-energy surface for dissociation of ion **1** seems straightforward. A methyl hydrogen and the fluorine come together in a four-center transition state. After passing this barrier, the two fragments part and pass over a potential-energy well that corresponds to a complex between HF and the 2-propenyl cation.[24] The DFT-calculated barrier top lies 267 kJ mol^{-1} above **1**, which accounts for the large translational kinetic-energy release that is seen in Figure 1. The calculated net endothermicity, 184 kJ mol^{-1} (which includes a counterpoise correction for basis set superposition error), implies a reverse activation barrier of 83 kJ mol^{-1}.

The products of the elimination, 2-propenyl cation and HF, lie in a potential-energy well that is 63 kJ mol^{-1} deep. Topological analysis of the electron density shows that a pair of hydrogen bonds, one from a methyl CH and the other from a methylene CH, to fluorine hold the $[CH_3C{=}CH_2^+\cdots FH]$ complex together, as drawn in Figure 6. These hydrogen bonds correspond to the two different neutral products that could form from the deprotonation of the 2-propenyl cation, allene and propyne, respectively. Despite the presence of the well on the potential surface, the dish-topped metastable peaks in Figure 1 indicate that the elimination passes directly to the products without sojourning in this well.

The calculated potential-energy surface for ion **4** requires more detail. Given that scrambling of isotopic label takes place, HF elimination can occur via either a four-membered transition state that is analogous to the one in Figure 6 or a five-membered transition state from the intermediate that is responsible for the interchange of methyl and ring hydrogens. Before considering HF expulsion from **4** in further detail, an examination of the pathway for its unimolecular hydrogen scrambling is warranted. The most plausible mechanism involves proton transfer from the methyl group to the ring to form fluorostyrene protonated at the ortho position, followed by a series of transpositions that equilibrate the six hydrogens. The initially formed structure is drawn at the center of Figure 7 and will be designated as possessing the syn orientation of the C=C double bond relative to the protonated ring position. This isomer lies 98 kJ mol^{-1} above **4**.

Once formed, protonated fluorostyrenes can rearrange via two pathways. On one hand, the $CF{=}CH_2$ group can rotate 180°, so as to put the C=C double bond anti to the protonated ring position (the structure drawn to the left in Figure 7). The transition state for this rotation lies 44 kJ mol^{-1} above the syn-ortho structure. The resulting anti-ortho orientation (the geometry from which HF elimination can subsequently take place) has an energy that is 6 kJ mol^{-1} lower than that of the syn-ortho orientation. On the other hand, protons can migrate around the ring via a sequence of 1, 2 shifts. The highest barrier corresponds to the isomerization of the syn-ortho to the syn-meta isomer. That step has a calculated barrier of 67 kJ mol^{-1}. The syn-meta is the least stable of the ring-protonated fluorostyrenes (apart from the ipso-protonated isomer, which does

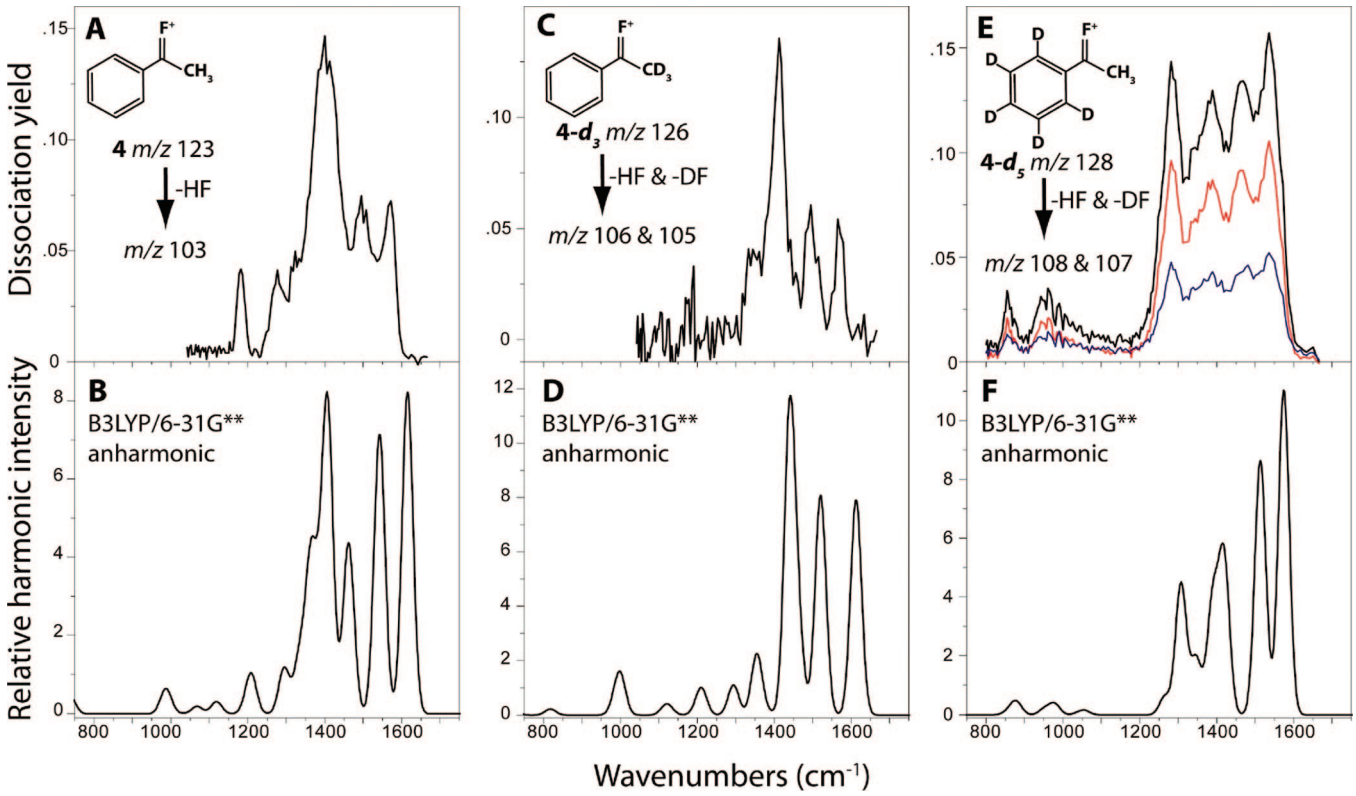

Figure 4. IRMPD spectra (upper panels) and DFT-predicted absorption bands (lower panels; 30 cm^{-1} fwhm Gaussian line shape) of $PhCFMe^+$ ions (**4**, **4**-d_3, and **4**-d_5) produced from PhCOMe-d_0, -d_3, and -d_5 via eq 2. Colored traces in panel E show the action spectra for DF (red) and HF (blue) losses separately.

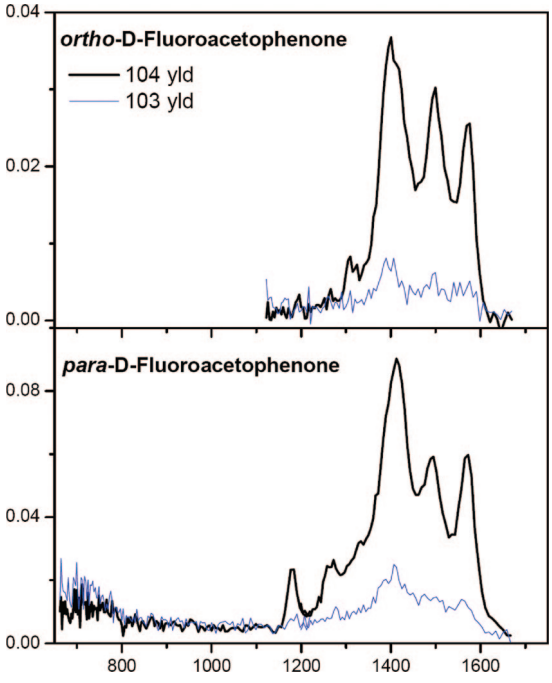

Figure 5. IRMPD spectra of isomeric monodeuterated $PhCFMe^+$ ions (**4**-*ortho*-*d* and **4**-*para*-*d*) that are produced by eq 2 via reactions of the corresponding monodeuterated acetophenones with CF_3^+. Black traces show the action spectra for HF loss, and blue traces show the action spectra for DF loss.

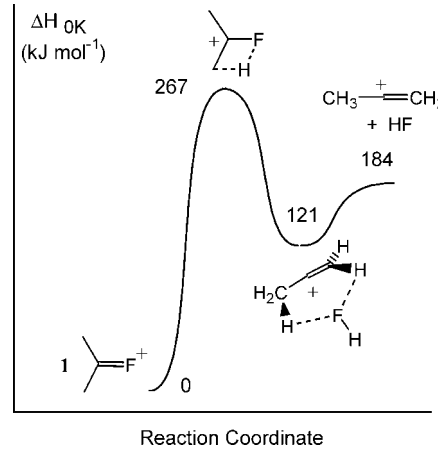

Figure 6. DFT reaction diagram (B3LYP/6-31G**) for HF expulsion from Me_2CF^+ (**1**) via a four-center transition state to produce the vinylic 2-propenyl cation $CH_3C{=}CH_2^+$.

not contribute to hydrogen scrambling) and has an energy that is 26 kJ mol^{-1} above that of the syn-ortho orientation.

Figure 8 compares stationary points that are calculated for the isomerization of **4** with the barriers for HF expulsion. Expulsion of HF has a calculated 0 K ΔH of 151 kJ mol^{-1}, which is 32 kJ mol^{-1} less endothermic than HF expulsion from **1**. Nevertheless, the four-center transition state, TS1, has a much higher barrier, $\Delta H^{\ddagger} = 301$ kJ mol^{-1}, than does the corresponding transition state for HF expulsion from ion **1**, $\Delta H^{\ddagger} = 267$ kJ mol^{-1}. This unexpected result can be ascribed to the loss of resonance when the positive charge shifts out of conjugation with the benzene ring during the hydrogen transfer.

The transition state for transferring a methyl proton to the ring to form syn-ortho protonated fluorostyrene, TS2, is much lower ($\Delta H^{\ddagger} = 230$ kJ mol^{-1}). The isomerizations summarized in Figure 7 can then rapidly take place because they have even lower barriers. The subsequent transfer of a proton from the ring to fluorine in the anti-ortho structure (the orientation represented in Figure 8) can occur via a five-center transition

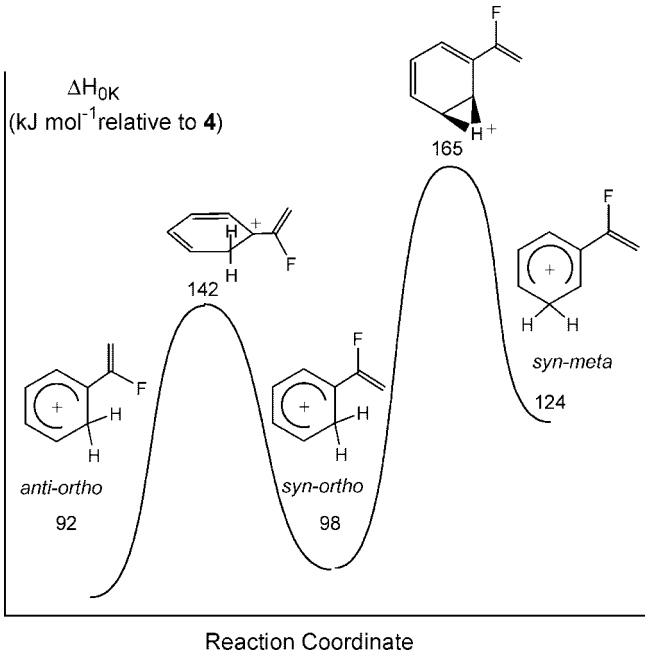

Figure 7. DFT reaction diagram for bond rotation and hydrogen shifts in ring-protonated α-fluorostyrene (**12**).

state, TS3, with concomitant expulsion of HF. The five-center TS3 lies 10 kJ mol^{-1} higher in energy than does TS2, but it is still 61 kJ mol^{-1} lower than TS1. Regardless of the pathway by which **4** loses HF, a [PhC=CH_2^+···FH] complex intervenes along the reaction coordinate. Only one hydrogen bond holds this complex together, and it lies in a well that is 23 kJ mol^{-1} deep relative to the final products.

The curves drawn in Figures 6−8 provide visual aids for connecting calculated stationary points, not computed reaction paths. Because the barrier height for dissociation (TS3) in Figure 8 lies above the one for internal proton transfer (TS2), it should be possible to excite $PhCFMe^+$ ions to the extent that they scramble hydrogens unimolecularly without losing HF. Such an experiment remains to be attempted.

Equation 2 provides a highly energetic route to ions **4** (calculated by DFT to be exothermic by $\Delta H = -324$ kJ mol^{-1}). Nevertheless, the IRMPD spectra demonstrate that transposition of label does not occur to a detectable extent prior to excitation. This outcome can be ascribed to the comparatively narrow energy difference that separates TS2 and TS3. The partitioning of the exothermicity between the two products tends to impart either so much internal energy to the ion that it spontaneously further dissociates to $C_8H_7^+$ (which is observed as a product of the ion−molecule reaction) or so little that the ion cannot surmount the barrier to internal proton transfer.

Discussion

The representation >C=F^+ confers a complete octet on both atoms. Therefore, Chart 1 depicts such ions as having carbon−fluorine double-bond character. Chemical intuition suggests that the simultaneous conjugation of the charge with a benzene ring should weaken a >C=F^+ linkage. A corollary suggests that such conjugation might also lower the barrier for elimination of HF. Results presented here (further discussed below) unexpectedly turn out to contradict this latter hypothesis.

As previously reported, the comparison of ions **2** and **3** shows that the conjugation of >C=F^+ with one double bond does not diminish the force constant for the CF stretch.[7] In general, three measures gauge the strength of a CF bond: bond length (r_{CF}), bond order (n), and stretching frequency. The adiabatic stretching mode ν_{CF} represents the pure CF component extracted from a set of normal vibrations for a molecule[13−16] and provides the last of the aforementioned assessments of bond strength. The degree of correlation among these three separate approaches (as summarized in Table 1) confirms that an α-fluorinated carbocation has a CF bond order that is substantially greater than 1. The AIM method assigns CF bond orders in the n = 1.3 to 1.4 range for aliphatic cations.

Figure 2 gives an idea of how conjugation with an aromatic ring affects CF bond strength. CF bonds elongate, and their bond orders fall below n = 1.3. Likewise, adiabatic CF stretching modes become looser. For instance, ν_{CF} for ion **4** has a value that is 100 cm^{-1} lower than that for ion **1**. Protonated fluorobenzene **8** (whose gas-phase IRMPD spectrum has been reported[25]) shows a value that is 50 cm^{-1} lower than that of **1** but 120 cm^{-1} higher than that of neutral fluorobenzene **9**. Difluorinated ion **11** (whose IR spectrum in the crystalline phase has been reported[26]) can delocalize positive charge onto both fluorines; both of its ν_{CF} values lie between those for **8** and **9**.

Experimental evidence supports the conclusion that ion **4** can be produced in the gas phase without forming isomeric ions. Expulsion of neutral HF serves as the sole pathway for its dissociation when the ion is activated. DFT gives a good fit to the IR spectra of **4** and its deuterated analogues, particularly in the 1200−1600 cm^{-1} domain, where the strongest absorptions are observed. Observation of a characteristic absorption pattern for each deuterated analogue demonstrates that the labeling pattern of the ion is the same as that of its neutral precursor. However, once the ion has been activated in the course of IRMPD, scrambling of the isotopic label occurs prior to ion decomposition.

The observed agreement between theoretical and observed vibrational spectra confirms the inference that the >C=F^+ bond in **4** is weaker than that in ions **1**−**3**. This does not necessarily imply a lower barrier to ion dissociation. MIKE spectra indicate two pathways for dissociation: a minor pathway with a large translational kinetic-energy release (which gives rise to barely discernible dish-topped peaks underneath much larger Gaussian peaks) and a major pathway, which exhibits translational kinetic-energy release values of $T_{0.5}$ = 0.03 eV.

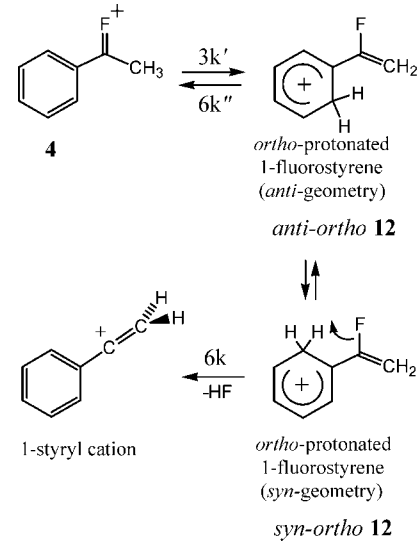

(5)

Equation 5 represents the major pathway inferred for the dissociation of **4**. The rate coefficients k, k', and k″ are given

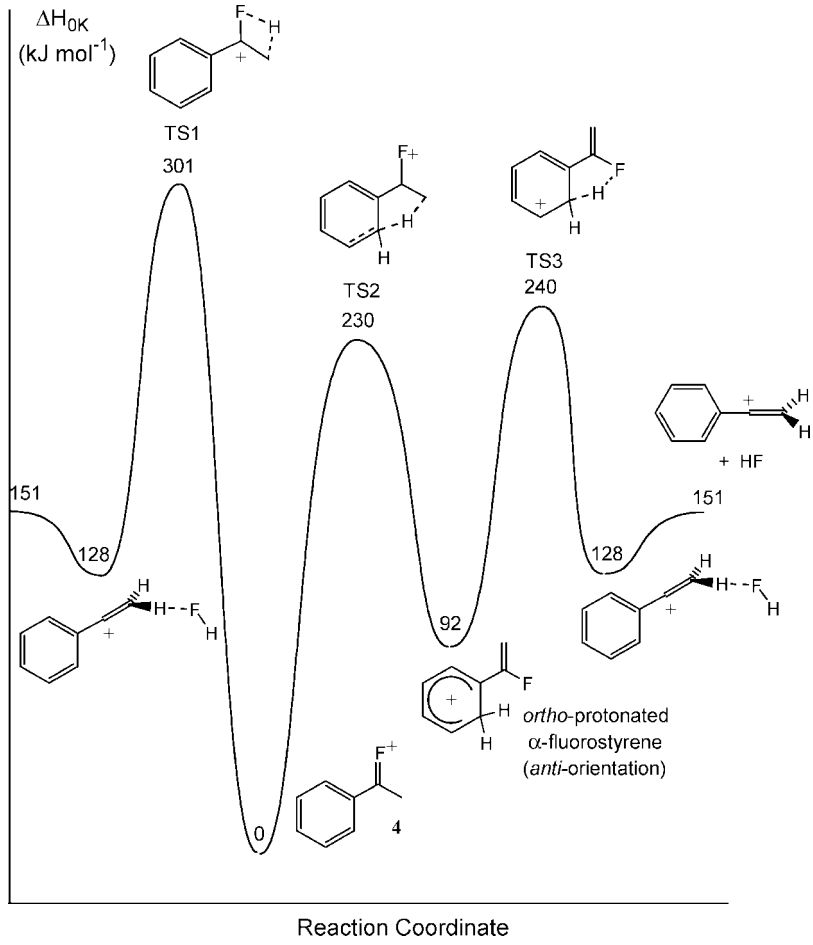

Figure 8. DFT reaction diagram for competition among tautomerization and four- and five-center HF expulsion pathways for $PhCFMe^+$ (**4**).

statistical weights that are proportional to the number of protons that can participate. In particular, the weights of k and k″ reflect the supposition that all six hydrogens randomize within a protonated benzene ring.[27] Assuming that contributions from the very small dish-topped components can be neglected, relative rate coefficients can be extracted from the experimental ratios of HF loss to DF loss in the MIKE spectra in Figure 3, provided that two additional assumptions are made. The first requires that the metastable ion product distribution can be fitted by the use of first-order kinetics with a steady-state approximation. The second stipulates that scrambling takes place via the shift of one methyl proton to the benzene ring, followed by the randomization of all six hydrogens that are now attached to the ring, as eq 5 illustrates. The precedent for this latter supposition comes from studies of other protonated benzenoid systems in which reported studies have confirmed isotopic randomization.[27]

Scheme 1 depicts a mechanism by which a hydrogen, once transferred from the methyl group to the ring of ion **4-*d*$_3$**, can equilibrate completely with the other ring hydrogens. This pathway does not necessitate that all three methyl hydrogens randomize with the ring hydrogens (which would not agree with the relative peak intensities observed in the MIKE spectra). Instead, Scheme 1 supposes that the deuteron rapidly moves around the ring in the protonated fluorostyrene ions **13** (as well as forms other tautomers that are not shown) prior to dissociation. The theory predicts that, as Figures 6 and 7 portray, 1, 2 shifts within the ring encounter barriers that are much lower than those for HF or DF elimination.

Species **13** in Scheme 1 illustrate just some of the isomers that become accessible after **4-*d*$_3$** tautomerizes to ring-protonated

SCHEME 1: Mechanism by Which Methyl Hydrogens Randomize One at a Time with Ring Hydrogens

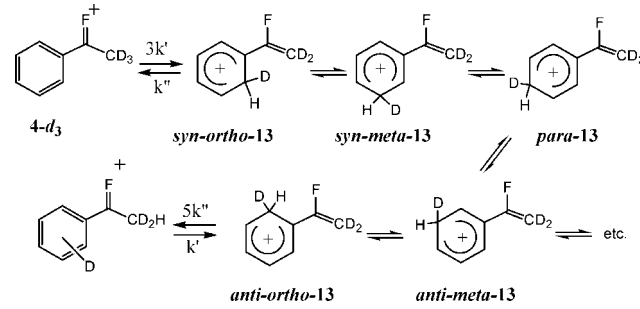

fluorostyrenes. After a methyl hydrogen has transferred to the ring, it randomizes completely with the ring hydrogens. The statistically weighted rate coefficients k' and k'' correspond to the transfers of a deuteron from the methyl to the ring and of a proton from the ring to the methylene. Isotope effects on these rate coefficients are assumed to be negligible; that is, k' and k'' for the transfer of D^+ are taken to be the same as those for the transfer of H^+. Although an assumption of this nature (needed because of the limited number of data) introduces systematic error to the result, it permits a comparison with the isotope effects of HF/DF loss from $CH_3CFCD_3^+$ (Figure 1C) versus eq 5.

As stated above, precedent supports the supposition that all six ring-hydrogens completely randomize once ion **13** forms. Scheme 2 summarizes the overall picture for **4-*d*$_5$**, which is drawn as structure A. Internal H^+/D^+ transfers are reversible, as in Scheme 1. After tautomerization of $PhCFMe^+$ to a ring-

SCHEME 2: Competition between HF/DF Loss and Transposition of Hydrogen from the Methyl to the Ring

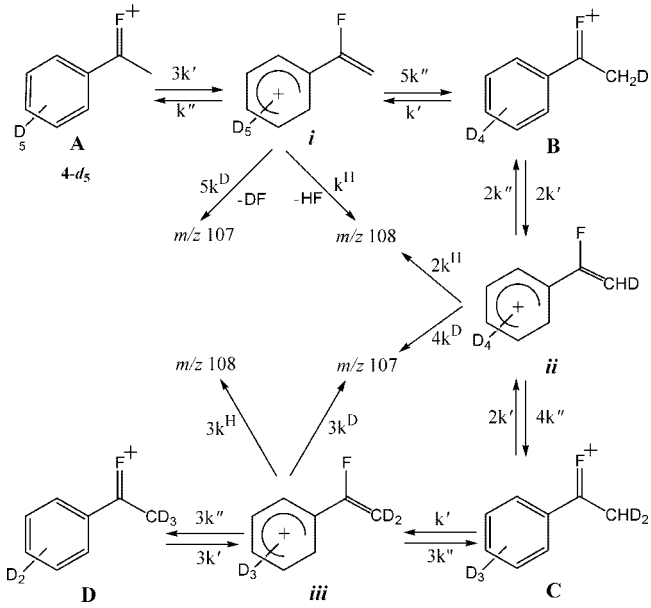

TABLE 2: Fragment Ion Abundance Ratios for HF/DF Losses from Deuterated $PhCFMe^+$ Parent Ions for Two Different Metastable Ion-Decomposition Time Windows and Corresponding Values for Relative Rates Extracted by the Use of Steady-State, First-Order Kinetics Analysis[a,b]

	m/z 107:108 from **4-*d*$_5$**	*m/z* 105:106 from **4-*d*$_3$**	k^H/k^D	k''/k^D
B/*E*	1.52 ± 0.01	0.317 ± 0.012	1.43	6.37
MIKES	1.58 ± 0.04	0.293 ± 0.011	1.46	5.13

[a] Fragment ion abundance ratios based on relative areas of curve fitting routines; error bars represent 95% confidence limits. [b] Relative rates based on Schemes 1 and 2.

protonated fluorostyrene, elimination of HF or DF (symbolized by the rate coefficients k^H and k^D) competes with the return to the $PhCFMe^+$ structure (symbolized by rate coefficient k'').

In each stage, the ring-protonated fluorostyrenes *i*−*iii* are assumed to randomize the six hydrogens in the ring. By using the steady-state approximation, we can extract two relative rate coefficients, k^H/k^D for the metastable decomposition and k''/k^D (the ratio of the back exchange rate to the rate of DF loss), from the two ratios of peak areas in Figure 3B,C. Whereas the kinetic analysis is approximate (given the assumptions on which it is based), it clearly indicates that k^H/k^D has a substantially smaller value for eq 5 than it does for HF versus DF elimination from Me_2CF^+. Table 2 lists experimental ratios of peak areas and the relative rate coefficients extracted from them by a steady-state analysis of competing first-order reactions.

Mass spectrometric dissociations of monoenergetic ions exhibit first-order kinetics, but ensembles that contain ions with a range of internal energies need not do so.[28] Conditions under which steady-state, first-order schemes provide a valid approximation for analyzing competing reactions have been described.[29] In terms of Scheme 2, for instance, these conditions correspond to the limit in which the *m/z* 107:108 intensity ratio averaged over the domain of energies sampled in the window is the same as the weighted average *m/z* 107 intensity divided by weighted average *m/z* 108 intensity sampled over the same domain.

We propose that the examination of two different time windows offers an empirical test of whether those conditions are met. Consider two ratios of rate coefficients: one (such as an isotope effect in the absence of tunneling) that ought not to vary substantially with internal energy and the other (such as a branching ratio) that should display a greater dependence on internal energy. If analysis of fragment ion intensities in two different time windows shows that the former remains constant while the latter changes, then this outcome justifies the steady-state, first-order analysis of the data to extract the energy-independent relative rate. That is to say, a nonuniform internal energy distribution should not significantly distort an isotope effect.

The double-focusing mass spectrometer that was used for these experiments has two field-free regions (FFRs). In a reverse Nier−Johnson geometry (*B*/*E*), the first FFR intervenes between the ion source (where ions are all accelerated to the same kinetic energy) and mass selection by the magnetic (*B*) sector. The time window that corresponds to the first FFR starts 1 to 2 μs after ion formation and has a duration of approximately 3 μs for the *m/z* values that are under consideration here. First FFR metastable ion decompositions can be viewed by the use of a linked scan that holds *B*/*E* constant.

The second FFR intervenes between mass selection and energy selection by the electrostatic (*E*) analyzer. This time domain begins on the order of 10 μs after ion formation and lasts on the order of 10 μs. Other things being equal, ions that decompose in the first FFR have a greater internal energy than do those that decompose in the second FFR. As noted in Figure 3, second FFR metastable ion decompositions can be viewed using MIKE spectroscopy in which the magnetic sector has a fixed field that passes the parent ion while the electrostatic analyzer is scanned.

As Table 2 summarizes, the parent ion dissociates ca. 20% faster in the first FFR (k'' relative to k^D) than in the second FFR. In contrast, k^H/k^D changes by ∼2%, a difference that is not significant. From this analysis, we conclude that the value for the isotope effect on HF expulsion has a value of k^H/k^D = 1.45. This value is considerably smaller than the isotope effect for the four-center elimination from $CD_3CFCH_3^+$, whose metastable dissociations are shown in Figure 1C.

The trend in experimental isotope effects qualitatively agrees with DFT predictions. The transition state for DF elimination from $CD_3CFCH_3^+$ has a calculated harmonic zero-point energy difference (ΔZPE) that is 4.30 kJ mol^{-1} greater than that for HF elimination. The anharmonic value does not differ substantially (ΔZPE =4.37 kJ mol^{-1}). For the elimination of DF versus that of HF via five-center transition states from ***anti-ortho*-13**, ΔZPE = 3.86 kJ mol^{-1}. The change in observed isotope effects (k^H/k^D = 4 in Figure 1C vs k^H/k^D = 1.45 in Table 2) is more pronounced than that which might have been anticipated on the basis of DFT calculations, but theory does correctly predict the decrease in k^H/k^D in going from the four-center to the five-center transition state.

Conclusions

Two mechanisms are described by which aromatic α-fluorinated carbocations can eliminate HF to yield vinylic cations. One pathway proceeds directly via a four-center transition state and gives rise to a large translational kinetic-energy release. This is the only pathway seen for simple aliphatic ions such as **1**. The other pathway operates via intramolecular proton transfer, followed by elimination via a five-center transition state, and it exhibits a much smaller translational kinetic-energy release. This pathway dominates the metastable ion decompositions of ions such as **4** in which the positive charge is conjugated with an

aromatic ring. In this case, the dissociation via the four-center transition state contributes a barely detectable component.

Theory and experiment both demonstrate that CF bonds in α-fluorinated carbocations become weaker when the positive charge delocalizes into a benzene ring; nevertheless, the bonds are considerably shorter and stronger than those in neutral molecules. Theory does not support the supposition that the four-center decomposition pathway enjoys a lower barrier as a consequence of bond weakening. However, theory does suggest that the five-center HF loss encounters a lower barrier than does the four-center HF loss but not by more than a 20% difference.

Isotopic labels remain in the same positions in $PhCFMe^+$ ions (**4** and its isotopomers) as they do in their neutral precursors until the ion becomes sufficiently activated. The dominant five-center pathway for HF elimination proceeds via protonated fluorostyrene intermediate **12**, which rapidly transposes hydrogens internally prior to dissociation. The calculated threshold for HF expulsion is 10 kJ mol^{-1} higher than the barrier for the isomerization to **12**; therefore, the loss of both HF and DF occurs from all of the partially deuterated $PhCFMe^+$ ions. Experimental data do not support the interpretation that complete randomization of all eight hydrogens takes place before the activated ion expels HF. Given reasonable assumptions about the pathway for isotopic scrambling in vibrationally excited ions, the rate of hydrogen transposition relative to expulsion for vibrationally excited unlabeled **12** is inferred to be $k''/k^H = 3.5$ to 4.5, depending on the internal energy. The deuterium isotope effect for the expulsion from deuterated analogues (such as **13**) displays much less sensitivity to internal energy and has a value on the order of $k^H/k^D = 1.45$.

The development of positron emission tomography (PET) as a biological imaging technique has raised the question of whether electrophilic reactions can be used to produce radiolabeled compounds with high specific activity.[30] The present results demonstrate that exceedingly exothermic gas-phase metatheses such as eq 2 can give rise to ions with well-defined structures, some of which have high barriers to further rearrangement or decomposition. The possibility that gas-phase ion chemistry might have an application in the preparation of radiofluorinated molecules presents an intriguing prospect.

Experimental Section

Gaseous $PhCFMe^+$ ions for unimolecular metastable ion decomposition studies were prepared from neutral fluorocumenes via EI, as shown in eq 1. Fluorocumenes were freshly synthesized by reaction of the corresponding alcohols with diethylaminosulfur trifluoride (DAST, Aldrich) and were directly used without further purification. The d_6 precursor $C_6H_5C(CD_3)_2OH$ of the trideuterated ion (**4-*d*$_3$**) shown in the second panel in Figure 3 was made by the addition of excess methyl-d_3 magnesium iodide (Aldrich) to benzoyl chloride. The d_5 precursor $C_6D_5C(CH_3)_2OH$ of the pentadeuterated ion (**4-*d*$_5$**) shown in the third panel in Figure 3 was made by the addition of methylmagnesium iodide to commercial acetophenone-d_5 ($C_6D_5COCH_3$, Fluka).

IRMPD spectra were conducted on ions prepared in an ICR cell via gas-phase reactions of the corresponding neutral acetophenones with ions produced by EI on CF_4 in an external ion source. Commercial acetophenone-d_5 and -d_3 (Fluka) were used to make **4-*d*$_5$** and **4-*d*$_3$**, respectively. We prepared the isomeric monodeuterated acetophenone precursors to ions **4-*ortho-d*** and **4-*para-d*** by heating commercial samples of *ortho*-bromoacetophenone and *para*-bromoacetophenone, respectively, with tri-*n*-butyltin deuteride (Aldrich), a reaction that produced approximately as much undeuterated acetophenone as d_1 product. The separate identities of isomeric monodeuterated acetophenones were ascertained by means of proton-decoupled ^2H NMR spectra, which showed them to have different chemical shifts and each to contain a single monodeuterated compound.

Spontaneous metastable ion decomposition experiments were conducted on a reverse Nier−Johnson (*B*/*E*) double-focusing mass spectrometer using 70 eV EI. Fragment ions from the methyl loss of ionized fluorocumenes were either mass selected and allowed to dissociate in the second FFR (MIKE spectra) or analyzed by means of fixed-ratio *B*/*E* scans. MIKES peaks were deconvolved as Gaussian profiles of variable widths by the use of IGOR Pro software (Wavemetrics, Lake Oswego, OR), and relative abundance ratios for HF and DF losses were determined from the relative areas of the Gaussian profiles. We measured the areas of the *B*/*E* peaks by fitting the profiles using Voigt functions. The sets of differential equations for Scheme 2 and the corresponding scheme for **4-*d*$_3$** were solved by the use of Mathematica.

IR resonant multiphoton dissociation experiments were conducted in a Fourier transform ion cyclotron resonance (FTICR) mass spectrometer coupled to the infrared beam line of FELIX, the free-electron laser for infrared experiments at Rijnhuizen. Details of the laser, the FTICR, and the multiphoton dissociation process are described elsewhere.[8f] Briefly, CF_4 was leaked into an external ionization chamber at a pressure of $\sim 3 \times 10^{-5}$ Torr, and the fragment ions were injected into the ICR cell. A He gas pulse was then used to capture ions and to cool them collisionally. The ionizer was a slightly modified Micromass EI/CI source with a tungsten filament using an electron energy typically around 60 eV. The fragment ions (principally CF_3^+) were injected into the ICR cell of a home-built 4.7 T FTICR mass spectrometer via a quadrupole deflector and a 1-m-long RF octopole ion guide. A transient pressure of He from a gas bulb was then introduced into the ICR cell via a pulsed valve. The gas bulb contained approximately 1 atm of helium with a few Torr partial pressure of ketone. Partial pressures of acetophenones in the gas bulb and the duration of the gas pulse were adjusted so as to optimize the abundance of $PhCFMe^+$ ions, which undergo rapid deprotonation by ion–molecule reactions with neutral ketone after they are formed. With unlabeled acetophenone added to the He gas, the methathesis reaction (eq 2) between CF_3^+ and $C_6H_5COCH_3$ yields the *m*/*z* 123 ion. After a 3 s pump and cooling delay, the $PhCFMe^+$ ions were mass isolated by the use of a SWIFT excitation pulse,[31] which removed the remaining CF_3^+, the reaction products from HF/DF expulsion, the protonated PhCOMe, and other unwanted ions. In this fashion, for example, it was possible to obtain essentially pure $C_6H_4DCFCH_3^+$ ions (*m*/*z* 124) from the monodeuterated acetophenone precursors despite the presence of undeuterated acetophenone as a contaminant. Subsequently, a mechanical shutter opened, which exposed the ions to the IR radiation of FELIX,[8a] in which 30 macropulses were typically accumulated (6 s of irradiation). When the laser wavelength is in resonance with an allowed vibrational transition in the ion, multiple photon absorption occurs by virtue of the high pulse energy of the FEL (typically 30 mJ in a 5 μs pulse). Incoherent, IVR-mediated multiple-photon excitation[32] allows each ion to absorb on the order of 10−100 IR photons, and the ions thereby reach internal energies that are substantially above the dissociation threshold.[33] A standard FTICR excite/detect sequence then determined the amount of parent and fragment ions (e.g., *m*/*z* 123 and 103, respectively, from the excitation of $C_6H_5CFCH_3^+$), and an action spectrum was generated by

plotting their ratio as a function of the IR wavelength. In the case of multiple dissociation pathways, fragment yields into the different channels were added to give the total IRMPD spectra that are reproduced in Figures 4 and 5.

Computational. Topological analyses of DFT wave functions were conducted by using the AIM approach,[34] as implemented by the AIM2000 computer code (SBK Software, http://www.aim2000.de). Electron densities at bond critical points (ρ_{BCP}) were used to calculate bond orders n, as previously described, by using the equation given in Table 1 to ensure that $n = 0$ when $\rho_{BCP} = 0$.[35]

Adiabatic vibrational modes were calculated with the program ADIA, which is part of the program package Cologne 2008.[18] Adiabatic mode vector $\mathbf{a}_n$ was calculated from normal mode coordinate Q_μ and its associated force constant k_μ, which are given in the internal coordinate space in the harmonic approximation. The adiabatic mode frequency ν_{adia} is given by

$$\nu_{adia} = \mathbf{a}_n^{+}\mathbf{F}\mathbf{a}_n G_{nn} = k_{adia} G_{nn} \quad (6)$$

where $\mathbf{F}$ is the force constant matrix for the normal vibrational modes, G_{nn} is an element of the Wilson $\mathbf{G}$ matrix, and k_{adia} is the adiabatic force constant. For more details, see refs 14−16.

Acknowledgment. This work was supported by NSF grants CHE0306515 and CHE0717893 and by the Nederlandse Organisatie voor Wetenschappelijk Onderzoek (NWO). We acknowledge the skillful assistance of the FELIX staff, in particular Dr. Britta Redlich, and the contribution of Dr. Dan Borchardt, who recorded ^{2}H NMR spectra.

Supporting Information Available: DFT energies, tabulated IRMPD band positions, and analysis of kinetic schemes. This material is available free of charge via the Internet at http://pubs.acs.org.

References and Notes

(1) van Alem, K.; Lodder, G.; Zuilhof, H. *J. Phys. Chem. A* **2002**, *106*, 10681–10690.

(2) Kiprof, P.; Miller, S. R.; Frank, M. A. *THEOCHEM* **2006**, *764*, 61–67.

(3) Ridge, D. P. *J. Am. Chem. Soc.* **1975**, *97*, 5670–5674.

(4) (a) Johnson, W. S.; Daub, G. W.; Lyle, T. A.; Niwa, M. *J. Am. Chem. Soc.* **1980**, *102*, 7800–7802. (b) Johnson, W. S.; Lyle, T. A.; Daub, G. W. *J. Org. Chem.* **1982**, *47*, 161–163.

(5) Christe, K. O.; Zhang, X.; Bau, R.; Hegge, J.; Olah, G. A.; Surya Prakash, G. K.; Sheehy, J. A. *J. Am. Chem. Soc.* **2000**, *122*, 481–487.

(6) Levin, R. H.; Weingarten, L. *Tetrahedron Lett.* **1975**, *16*, 611–614.

(7) Oomens, J.; Morton, T. H. *Angew. Chem., Int. Ed.* **2008**, *47*, 2106–2108, Force constants in the final paragraph of this article should read mdyne/Å

(8) (a) Oepts, D.; van der Meer, A. F. G.; van Amersfoort, P. W. *Infrared Phys. Technol.* **1995**, *36*, 297–308. (b) Lemaire, J.; Boissel, P.; Heninger, M.; Mauclaire, G.; Bellec, G.; Mestdagh, H.; Simon, A.; Caer, S. L.; Ortega, J. M.; Glotin, F.; Maître, P. *Phys. Rev. Lett.* **2002**, *89*, 273002. (c) Maître, P.; Le Caër, S.; Simon, A.; Jones, W.; Lemair, J.; Mestdagh, H.; Heninger, M.; Mauclaire, G.; Boissel, P.; Prazeres, R.; Glotin, F.; Ortega, J.-M. *Nucl. Instrum. Methods Phys. Res., Sect. A* **2003**, *507*, 541–546. (d) Chiavarino, B.; Crestoni, M. E.; Fornarini, S.; Lemaire, J.; MacAleese, L.; Maître, P. *ChemPhysChem* **2004**, *5*, 1679–1685. (e) Valle, J. J.; Eyler, J. R.; Oomens, J.; Moore, D. T.; van der Meer, A. F. G.; von Helden, G.; Meijer, G.; Hendrickson, C. L.; Marshall, A. G.; Blakney, G. T. *Rev. Sci. Instrum.* **2005**, *76*, 023103. (f) Polfer, N. C.; Oomens, J. *Phys. Chem. Chem. Phys.* **2007**, *9*, 3804–3817.

(9) Redman, E. W.; Johri, K. K.; Morton, T. H. *J. Am. Chem. Soc.* **1985**, *107*, 780–784.

(10) (a) Eyler, J. R.; Ausloos, P.; Lias, S. G. *J. Am. Chem. Soc.* **1974**, *96*, 3673–3675. (b) Ausloos, P.; Lias, S. G.; Eyler, J. R. *Int. J. Mass Spectrom. Ion Processes* **1975**, *18*, 261–271. (c) McEwan, M. J.; Wilson, P. F.; Francis, G. J.; Morton, T. H. *Int. J. Mass Spectrom.* **2007**, *267*, 81–88.

(11) Nguyen, V.; Mayer, P. S.; Morton, T. H. *J. Org. Chem.* **2000**, *65*, 8032–8040.

(12) Shaler, T. A. Ph.D. Thesis, University of California, Riverside, 1990.

(13) Cremer, D.; Larsson, J. A.; Kraka, E. New Developments in the Analysis of Vibrational Spectra. On the Use of Adiabatic Internal Vibrational Modes. In *Theoretical Organic Chemistry*; Párkányi, C., Ed.; Elsievier: Amsterdam, 1998, *Vol. 5*, pp 259−329.

(14) (a) Konkoli, Z.; Cremer, D. *Int. J. Quantum Chem.* **1998**, *67*, 1–10. (b) Konkoli, Z.; Larsson, J. A.; Cremer, D. *Int. J. Quantum Chem.* **1998**, *67*, 11–28. (c) Konkoli, Z.; Cremer, D. *Int. J. Quantum Chem.* **1998**, *6*, 29–40. (d) Konkoli, Z.; Larsson, J. A.; Cremer, D. *Int. J. Quantum Chem.* **1998**, *67*, 41–67.

(15) Larsson, J. A.; Cremer, D. *J. Mol. Struct.* **1999**, *485/486*, 385–407.

(16) Cremer, D.; Wu, A.; Larsson, A.; Kraka, E. *J. Mol. Model.* **2000**, *6*, 396–412.

(17) (a) Cioslowski, J.; Liu, G.; Mosquera Castro, A. A. *Chem. Phys. Lett.* **2000**, *331*, 497–501. (b) Kurita, E.; Hiroatsu, M.; Ohno, K. *Spectrochim. Acta, Part A* **2004**, *60*, 3013–3023.

(18) Kraka, E.; Gräfenstein, J.; Filatov, M.; Wu, A.; Joo, H.; Izotov, D.; Gauss, J.; He, Y.; He, Z.; Polo, V.; Reichel, F.; Konkoli, Z.; Olsson, L.; Cremer, D. *Cologne 2008*; University of the Pacific: Stockton, CA, 2008.

(19) (a) de Azvedo, A. L. M. S.; Neto, B. B.; Scarminio, I. S.; de Oliviera, A. E.; Bruns, R. E. *J. Comput. Chem.* **1996**, *17*, 167–177. (b) Baker, J.; Pulay, P. *J. Comput. Chem.* **1998**, *19*, 1107–1204.

(20) Innocenti, F.; Zuin, L.; Costa, M. L.; Dias, A. A.; Goubet, M.; Morris, A.; Oleriu, R. I.; Stranges, S.; Dyke, J. M. *Mol. Phys.* **2007**, *105*, 755–769.

(21) Sverdlov, L. M.; Kovner, M. A.; Krainov, E. P. *Vibrational Spectra of Polyatomic Molecules*; Wiley: New York, 1974.

(22) Pyykkö, P.; Riedel, S.; Patzschke, M. *Chem.−Eur. J.* **2005**, *11*, 3511–3520.

(23) Lide, D. R., Jr.; Mann, D. E. *J. Chem. Phys.* **1958**, *29*, 914–920.

(24) Stams, D. A.; Johri, K. K.; Morton, T. H. *J. Am. Chem. Soc.* **1988**, *110*, 699–706.

(25) Dopfer, O.; Solca, N.; Lemaire, J.; Maître, P.; Crestoni, M. E.; Fornarini, S. *J. Phys. Chem. A* **2005**, *109*, 7881–7887.

(26) Douvris, C.; Stoyanov, E. S.; Tham, F. S.; Reed, C. A. *Chem. Commun.* **2007**, *114*, 1145–1147.

(27) (a) Kuck, D. *Int. J. Mass Spectrom.* **2002**, *213*, 101–144. (b) Schröder, D.; Loos, J.; Schwarz, H.; Thissen, R.; Dutuit, O. *J. Phys. Chem. A* **2004**, *108*, 9931–9937.

(28) (a) Fairweather, R. B.; McLafferty, F. W. *Org. Mass Spectrom.* **1970**, *4*, 221–227. (b) Ling, Y.; Lifshitz, C. *J. Phys. Chem. A* **1998**, *102*, 708–716, and references therein.

(29) Kondrat, R. W.; Morton, T. H. *Org. Mass Spectrom.* **1991**, *26*, 410–415.

(30) Ametamey, S. M.; Honer, M.; Schubiger, P. A. *Chem. Rev.* **2008**, *108*, 1501–1516.

(31) Marshall, A. G.; Wang, T. C. L.; Ricca, T. L. *J. Am. Chem. Soc.* **1985**, *107*, 7893–7897.

(32) Bagratashvili, V. N.; Letokhov, V. S.; Makarov, A. A.; Ryabov, E. A. *Multiple-Photon Infrared Laser Photophysics and Photochemistry*; Harwood Academic: Chur, Switzerland, 1985.

(33) Oomens, J.; Sartakov, B. G.; Meijer, G.; von Helden, G. *Int. J. Mass Spectrom.* **2006**, *254*, 1–19.

(34) Bader, R. F. W. *Atoms in Molecules: A Quantum Theory*; Clarendon: Oxford, England, 1994.

(35) Traeger, J. C.; Morton, T. H. *J. Am. Soc. Mass Spectrom.* **2004**, *15*, 989–997.

JP804706Z